Minimizing optical losses in monolithic perovskite/c-Si tandem solar cells with a flat top cell

Santbergen, Rudi; Mishima, Ryoto; Meguro, Tomomi; Hino, Masashi; Uzu, Hisashi; Blanker, Johan; Yamamoto, Kenji; Zeman, Miro

DOI
10.1364/OE.24.0A1288

Publication date
2016

Document Version
Final published version

Published in
Optics Express

Citation (APA)
Santbergen, R., Mishima, R., Meguro, T., Hino, M., Uzu, H., Blanker, J., Yamamoto, K., & Zeman, M. (2016). Minimizing optical losses in monolithic perovskite/c-Si tandem solar cells with a flat top cell. *Optics Express*, *24*(18), A1288-A1299. https://doi.org/10.1364/OE.24.0A1288

Research Article | Vol. 24, No. 18 | 5 Sep 2016 | OPTICS EXPRESS A1288

Optics EXPRESS

Minimizing optical losses in monolithic perovskite/c-Si tandem solar cells with a flat top cell

RUDI SANTBERGEN,[1,*] RYOTA MISHIMA,[2] TOMOMI MEGURO,[2] MASASHI HINO,[2] HISASHI UZU,[2] JOHAN BLANKER,[1] KENJI YAMAMOTO,[2] AND MIRO ZEMAN[1]

[1]*Photovoltaic Materials and Devices Laboratory, Delft University of Technology, Mekelweg 4, 2628CD Delft, Netherlands*
[2]*Photovoltaic & Thin Film Device Research Laboratories, Kaneka Corporation, 5-1-1 Torikai-Nishi, Settsu, Osaka 566-0072, Japan*
**r.santbergen@tudelft.nl*

Abstract: In a monolithic perovskite/c-Si tandem device, the perovskite top cell has to be deposited onto a flat c-Si bottom cell without anti-reflective front side texture, to avoid fabrication issues. We use optical simulations to analyze the reflection losses that this induces. We then systematically minimize these losses by introducing surface textures in combination with a so-called burial layer to keep the perovskite top cell flat. Optical simulations show that, even with a flat top cell, the monolithic perovskite/c-Si tandem device can reach a matched photocurrent density as high as 19.57 mA/cm^2.

OCIS codes: (350.6050) Solar energy; (040.5350) Photovoltaic; (310.0310) Thin films.

References and links

1. M. A. Green, K. Emery, Y. Hishikawa, W. Warta, and E. D. Dunlop, "Solar cell efficiency tables (version 48)," Prog. Photovolt. Res. Appl. **24**(7), 905–913 (2016).
2. P. Löper, S.-J. Moon, S. M. de Nicolas, B. Niesen, M. Ledinsky, S. Nicolay, J. Bailat, J.-H. Yum, S. De Wolf, and C. Ballif, "Organic-inorganic halide perovskite/crystalline silicon four-terminal tandem solar cells," Phys. Chem. Chem. Phys. **17**(3), 1619–1629 (2015).
3. C. Ballif, J. Werner, G. Nogay, A. Walter, J. Geissbuhler, J. P. Seif, F. J. Haug, S. de Wolf, B. Niesen, C. Allebe, D. Saccetto, M. Despeisse, S. J. Moon, S. Nicolay, and J. Bailat, "Silicon solar cells with passivated contacts and their application in high-efficiency perovskite/c-Si tandem solar cells," in *EUPVSEC* (2016), paper 2DO.16.6.
4. J. Werner, C. H. Weng, A. Walter, L. Fesquet, J. P. Seif, S. De Wolf, B. Niesen, and C. Ballif, "Efficient monolithic perovskite/silicon tandem solar cell with cell area > 1 cm2," J. Phys. Chem. Lett. **7**(1), 161–166 (2016).
5. S. Albrecht, M. Saliba, J. P. Correa-Baena, K. Jager, L. Korte, A. Hagfeldt, M. Gratzel, and B. Rech, "Towards optical optimization of planar monolithic peerovskite/silicon-heterojunction tandem solar cells," J. Opt. **18**(6), 064012 (2016).
6. B. Lipovsek, J. Krc, and M. Topic, "Optical model for thin-film photovoltaic devices with large surface textures at the front side," J. Microelectron. Electron. Components Mater. **41**, 264–271 (2011).
7. R. Santbergen and R. J. C. van Zolingen, "The absorption factor of crystalline silicon PV cells: A numerical and experimental study," Sol. Energy Mater. Sol. Cells **92**(4), 432–444 (2008).
8. D. Zhang, W. Verhees, M. Dorenkamper, W. Qiu, K. Bakker, A. Gutjahr, S. Veenstra, R. Gehlhaar, U.W. Paetzold, W. Soppe, I. Romijn, L.J. Geerlings, T. Aernouts, A. Weeber, "Combination of advanced optical modeling with electrical simulations for performance evaluation of practical 4-terminal perovskite/c-Si tandem modules," SiliconPV conference 2016, to be published in Energy Procedia.
9. M. Filipič, P. Löper, B. Niesen, S. De Wolf, J. Krč, C. Ballif, and M. Topič, "CH(3)NH(3)PbI(3) perovskite / silicon tandem solar cells: characterization based optical simulations," Opt. Express **23**(7), A263–A278 (2015).
10. D. Adachi, J. L. Hernández, and K. Yamamoto, "Impact of carrier recombination on fill factor for large area heterojunction crystalline silicon solar cells with 25.1% efficiency," Appl. Phys. Lett. **107**(23), 233506 (2015).
11. Z. C. Holman, A. Descoeudres, L. Barraud, F. Z. Fernandez, J. P. Seif, S. De Wolf, and C. Ballif, "Current losses at the front of silicon heterojunction solar cells," IEEE J. Photovolt. **2**(1), 7–15 (2012).
12. D. Zhang, I. A. Digdaya, R. Santbergen, R. A. C. M. M. van Swaaij, P. Bronsveld, M. Zeman, J. A. M. van Roosmalen, and A. W. Weeber, "Design and fabrication of a SiOx/ITO double-layer anti-reflective coating for heterojunction silicon solar cells," Sol. Energy Mater. Sol. Cells **117**, 132–138 (2013).

#269150 http://dx.doi.org/10.1364/OE.24.0A1288
Journal © 2016 Received 4 Jul 2016; revised 19 Aug 2016; accepted 22 Aug 2016; published 26 Aug 2016

Optics EXPRESS

13. N. J. Jeon, J. H. Noh, Y. C. Kim, W. S. Yang, S. Ryu, and S. I. Seok, "Solvent engineering for high-performance inorganic-organic hybrid perovskite solar cells," Nat. Mater. **13**(9), 897–903 (2014).
14. P. Löper, M. Stuckelberger, B. Niesen, J. Werner, M. Filipič, S. J. Moon, J. H. Yum, M. Topič, S. De Wolf, and C. Ballif, "Complex refractive index spectra of CH3NH3PbI3 perovskite thin films determined by spectroscopic ellipsometry and spectrophotometry," J. Phys. Chem. Lett. **6**(1), 66–71 (2015).
15. S. Albrecht, M. Saliba, J. P. Correa Baena, F. Lang, L. Kegelmann, M. Mews, L. Steier, A. Abate, J. Rappich, L. Korte, R. Schlatmann, M. K. Nazeeruddin, A. Hagfeldt, M. Gratzel, and B. Rech, "Monolithic perovskite/silicon-heterojunction tandem solar cells processed at low temperature," Energy Environ. Sci. **9**(1), 81–88 (2015).
16. J. P. Mailoa, C. D. Bailie, E. C. Johlin, E. T. Hoke, A. J. Akey, W. H. Nguyen, M. D. McGehee, and T. Buonassisi, "A 2-terminal perovskite/silicon multijunction solar cell enabled by a silicon tunnel junction," Appl. Phys. Lett. **106**(12), 121105 (2015).
17. H. Tan, P. Babal, M. Zeman, and M. Smets, "Wide bandgap p-type nanocrystalline silicon oxide as window layer for high performance thin-film silicon multijuntion solar cells," Sol. Energy Mater. Sol. Cells **132**, 597–605 (2015).
18. R. Santbergen, A. H. M. Smets, and M. Zeman, "Optical model for multilayer structures with coherent, partly coherent and incoherent layers," Opt. Express **21**(S2), A262–A267 (2013).

1. Introduction

With a record efficiency of more than 25% [1], crystalline silicon (c-Si) solar cells have nearly reached their practical efficiency limit. Solar cells based on $CH_3NH_3PbI_3$ (perovskite) more recently exceeded an efficiency of 20%, albeit on a small area and not stabilized [1]. Because c-Si and perovskite have different bandgaps, 1.1 eV and 1.6 eV respectively, a tandem device with a perovskite top cell and a c-Si bottom cell, has an efficiency potential of more than 30% [2]. This makes this tandem device structure very attractive, especially considering that only low-cost materials are required. However, because the integration of a perovskite top cell and a c-Si bottom cell is not trivial, a perovskite/c-Si tandem device with an efficiency exceeding the c-Si solar cell record efficiency has so far not been demonstrated experimentally.

Two main approaches for fabricating perovskite/c-Si tandem devices are described in literature. In the first approach a transparent perovskite top cell is deposited front-to-back onto a glass substrate. The finished top cell is then bonded to the c-Si bottom cell. The top and bottom cells are coupled optically, but not connected electrically. Because both cells each have their own external contacts this results in a *four-terminal* tandem device. The highest efficiency thus far reported for such a four terminal device is 25.2% [3]. Alternatively, the perovskite top cell can be deposited back-to-front, directly on top of the c-Si bottom cell. This creates a *monolithic* perovskite/c-Si tandem device of which the top and bottom cell are electrically connected in series. The highest efficiency thus far demonstrated by this type of monolithic tandem device is 21.2% [4].

An advantage of the four-terminal approach is that the top and bottom cells can be optimized and processed independently. In addition, the current of the top cell does not need to match the current of the bottom cell. This gives more flexibility in the design of the tandem device. On the other hand, an advantage of the monolithic approach is that it does not require lateral current collection at the rear of the top cell and front of the bottom cell. This means that the two transparent conductive layers there can be omitted. This results in lower parasitic absorption losses and a higher efficiency potential. In addition, the monolithic tandem approach is more compatible with existing module technology and can potentially result in lower module cost. Also the system cost can be lower as only one maximum power point tracker is required. This makes the monolithic perovskite/c-Si tandem an attractive architecture.

When making a monolithic perovskite/c-Si tandem device, it has proven difficult to fabricate a working perovskite top cell on a c-Si bottom cell with the usual anti-reflective front side texture. Especially process steps that require spin-coating are problematic. Not surprisingly, the above mentioned 21.2% record efficiency has been achieved with a flat c-Si bottom cell, i.e. based on a double side polished c-Si wafer. From optical viewpoint this is far

Optics EXPRESS

from ideal as flat solar cells generally suffer from reflection losses and also trap weakly absorbed light very poorly.

Previous studies have, to some extent, addressed the reflection losses by tuning layer thicknesses and thereby exploiting interference effects [4,5]. This optimization can be done using relatively simple optical models, based on the transfer-matrix method. However, relatively few optical simulation studies have focused on light trapping, e.g. by introducing light scattering surface textures. The main reason for this is that this requires much more advanced optical models that combine both wave optics and ray optics. One of the few models that can do this is the CROWM model developed at Ljubljana University [6]. Also the GENPRO4 model developed at Delft University of Technology can perform these calculations [7]. Besides combing wave optics and ray optics in a more flexible way, GENPRO4 has a unique feature that allows to decompose reflection losses into the contributions from each interface. It also has a fast current-matching algorithm for simulation of multi-junction solar cells. This makes GENPRO4 especially suitable for fast and accurate simulation of light trapping in the perovskite/c-Si tandem devices considered here.

Recently, Zhang et al. used GENPRO4 [8] and Filipic et al. used CROWM [9] to study the effect of light trapping in four-terminal perovskite/c-Si tandem devices. Filipic et al. [9] also simulated monolithic devices, but light trapping was implemented by placing the perovskite top cell on texture, which is difficult to realize in practice. In this paper we focus on a monolithic tandem architecture that can be realized in practice, i.e. with a flat perovskite top cell. Our goal is to maximize the photocurrent density of this architecture using the GENPRO4 optical model. Starting from a completely flat monolithic perovskite/c-Si tandem device, we systematically improve light trapping and reduce reflection losses by introducing a rear side texture, a front side texture smoothened by so-called burial layer and an anti-reflective coating. The photocurrent density of the final optimized flat top cell architecture is presented and compared to alternative perovskite/c-Si tandem architectures.

2. Simulation input and validation

Accurate simulation of perovskite/c-Si tandem devices requires accurate input regarding the optical properties (refractive index, extinction coefficient) of all layers and the morphology of all interfaces. The next sections give the input used for the c-Si bottom cell (section 2.1), the perovskite top cell (section 2.2) and the tandem devices (section 2.3).

2.1 c-Si solar cell

The c-Si bottom cell considered here is the silicon heterojunction solar cell by Kaneka Corporation with an efficiency of 25.1% [1,10]. This cell consists of a 160 μm thick n-type c-Si wafer, with two thin hydrogenated amorphous silicon (a-Si:H) layers on both sides. The front has an a-Si:H i/p stack and the rear has an a-Si:H i/n stack. In addition the cell has a transparent conductive oxide (TCO) front contact and reflective TCO/metal rear contact. The cell's measured external quantum efficiency (EQE) is shown in Fig. 1 (red circles) [1].

The refractive index and extinction coefficient of all materials needed for optical simulation of this c-Si cell were measured in-house using spectroscopic ellipsometry. The morphology of the pyramid texture used in the simulation was measured using atomic force microscopy. The simulated absorptance in the c-Si wafer is shown in Fig. 1 (black line). Under the assumption that every absorbed photon generates one electron-hole pair and recombination is negligibly small, this absorptance is equivalent to the EQE. Note that here we included the small contribution from the absorptance in the front a-Si:H i-layer [11,12]. The corresponding short-circuit current density J_{sc}, calculated by integrating the EQE over the AM1.5 spectrum, is given in the legend of Fig. 1. The measured and simulated EQE show excellent agreement. This indicates that our optical model GENPRO4 can be used to predict the EQE and J_{sc} of this type of device. Although it would be interesting to calculate solar cell *efficiencies*, the additional electrical input parameters needed to simulate the current-voltage

Optics EXPRESS

characteristics (V_{oc} and FF) add much complexity and uncertainty. In this paper we therefore limit ourselves to maximizing the solar cells' J_{sc}, which can be done using purely optical simulations.

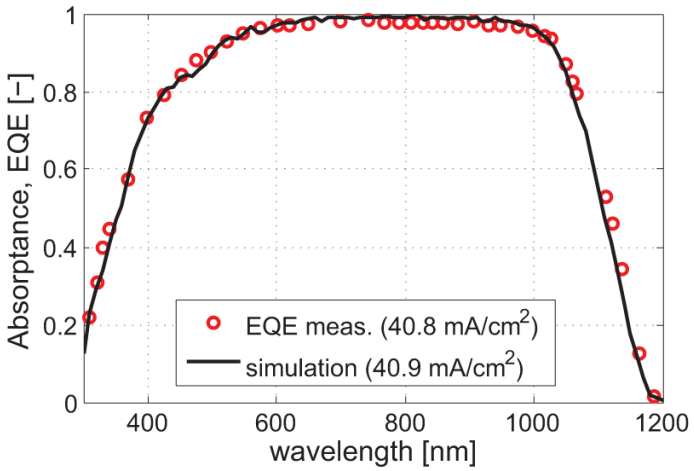

Fig. 1. The measured EQE (red circles) [1] and simulated absorptance in c-Si (black line) of the Kaneka c-Si heterojunction solar cell.

2.2 Perovskite solar cell

The fabrication of the perovskite solar cell starts with a glass/ITO substrate. Onto this, the electron transporting material (ETM), perovskite, hole transporting material (HTM) and ITO back contact are deposited. For simplicity, we will not consider the thin buffer layer (e.g. of MoO_x) that is usually present between HTM and ITO because it does not have a large optical effect. The ETM is compact TiO_2, deposited by vacuum deposition at a temperature less than 200°C, which in case of a tandem device is compatible with the underlying c-Si heterojunction solar cell. The perovskite layer is deposited by the solvent engineering method [13]. The HTM is poly(tri-arylamine) (PTAA), which is deposited by spin coating. In order to determine the optical properties of the ETM, perovskite and HTM layers, individual layers on a flat glass or c-Si substrates were prepared. From this, the optical properties were derived using spectroscopic ellipsometry and reflection transmission measurements. The resulting refractive index n and extinction coefficient k are shown in Fig. 2(a) and 2(b). This shows that the ETM (TiO_2, green line) has a refractive index around 2.3 and is highly transparent. This is in good agreement with the optical properties typically found for TiO_2 films deposited by vacuum deposition. The HTM (PTAA, blue line) has a lower refractive index around 1.7 and for wavelengths less than 400 nm its extinction coefficient is relatively high (> 0.1), which is in line with expectations. Perovskite (red solid line) has a refractive index that varies between 1.5 and 2.8. Its extinction coefficient reveals that it is highly absorbing up to a wavelength of 800 nm and much less absorbing for larger wavelengths. The n and k of perovskite from Löper et al. [14] are given for comparison (red dashed lines). Our refractive index follows a similar trend but for most of the spectrum is somewhat lower than the data from Löper et al. Our extinction coefficient on the other hand is somewhat higher than reported in literature. In addition we observe some sub-gap absorption that becomes stronger with increasing wavelength. We attribute this to free-carrier absorption. Photons absorbed by free carriers do no generate electron hole pairs and do not contribute to solar cell current. This sub-gap absorption therefore is a parasitic absorption loss.

Optics EXPRESS

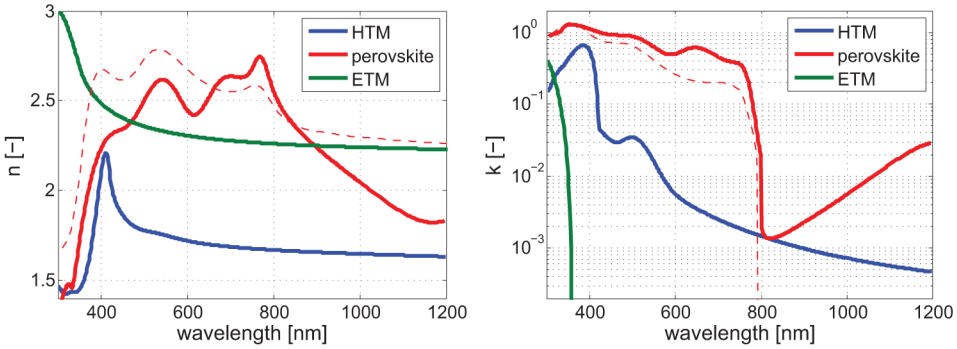

Fig. 2. Measured optical constants of HTM (blue), perovskite (red) and ETM (green). Optical constants of perovskite from literature [14] are given as red dashed lines. a) refractive index n, b) extinction coefficient k.

2.3 Perovskite/c-Si tandem device

The structure of the monolithic perovskite/c-Si tandem device is shown in Fig. 3(a). The perovskite cell is deposited back-to-front on top of the c-Si bottom cell. To match the polarity of the top and bottom cells the ETM is deposited first, followed by perovskite, HTM and finally the ITO front contact. Because top and bottom cell are electrically connected in series, the current of the tandem device is limited by the cell with the lowest current. Increasing the perovskite thickness increase the top cell current at the expense of the bottom cell current. The device current therefore reaches its maximum value when the top cell current exactly matches the bottom cell current. In all our simulations the thickness of the perovskite layer is varied such that the currents of top and bottom cell are perfectly matched in each configuration. The thickness of all other layers is fixed and their values are shown in Fig. 3(a).

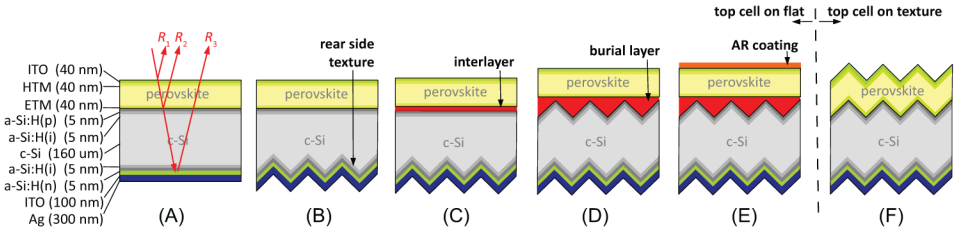

Fig. 3. Perovskite/c-Si tandem devices A to F. The layer thicknesses and the reflection losses R_1, R_2 and R_3 are indicated in Fig. (A).

3. Simulation results

In this section simulation results of the perovskite/c-Si tandem devices A to F, shown in Fig. 3, will be presented. Starting from the flat device A, the reflection losses R_1, R_2 and R_3 from the front, middle and rear of the tandem device, respectively (see Fig. 3(a)) will be addressed. Device B has a rear side texture to reduce R_3. Devices C and D use an additional interlayer or front side texture with burial layer to reduce R_2. Device E has an additional MgF_2 anti-reflective coating to reduce R_1. Finally, device F is similar to device B, but with front side texture. Note that devices A to E have a flat perovskite solar cell and can be fabricated easily with available technology. Device F suffers from the above mentioned fabrication issues and is difficult to fabricate.

Optics EXPRESS

3.1 Tandem with flat wafer (A)

First the perovskite/c-Si tandem cell with a *flat* c-Si cell (device A, shown in Fig. 3(a)) is simulated. The resulting absorptance versus wavelength is shown in Fig. 4. The light orange area indicates the useful absorptance in the absorber layers. The green and red lines show the individual absorptances from perovskite and c-Si layers, which we assume to be equivalent to the EQE of the top and bottom cell, respectively. By integrating these curves over the AM1.5 spectrum the implied photocurrent density is calculated. A perovskite thickness of 140 nm is required to obtain perfectly matched top and bottom cell current densities of 17.28 mA/cm^2. The other colored areas indicate the parasitic absorptance in other layers such as ITO (blue area at wavelength $\lambda < 400$ nm), HTM (yellow area at $\lambda < 400$ nm) or free carrier absorption in perovskite (green area at $\lambda > 1100$ nm). The absorption in other layers such as ETM, a-Si:H or back contact is small and not visible in the figure. The white area indicates the total reflectance. A unique feature of the GENPRO4 simulation tool is that it can decompose this total reflectance into the individual contributions R_1, R_2 and R_3, indicated in Fig. 3(a). R_1 represents the reflectance from all interfaces above the perovskite layer, R_2 represents the reflectance from all interfaces between perovskite and c-Si layer and R_3 represents the reflectance from all interfaces below the c-Si layer. A standard simulation gives reflectance $R_1 + R_2 + R_3$. A simulation of the same device but with an infinitely thick *c-Si* layer gives reflectance $R_1 + R_2$ and a simulation with an infinitely thick *perovskite* layer gives reflectance R_1. The white area in Fig. 4 is divided into three parts, representing R_1, R_2 and R_3, respectively. This reveals that R_1 is especially dominant for the shorter wavelengths. R_2 occurs only where the perovskite layer is transparent ($\lambda > 700$ nm) and is fairly constant around 7%. R_3 occurs only where both perovskite and c-Si are transparent ($\lambda > 950$ nm), but reaches a high value, up to 80%.

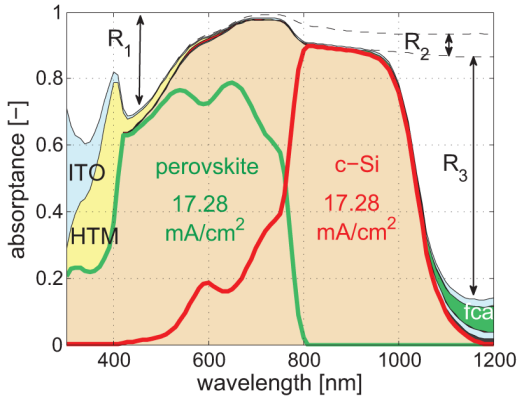

Fig. 4. Simulated absorptance and reflectance of current matched perovskite/c-Si tandem device A.

As an aside, this simulation is repeated using the *n* and *k* of perovskite from Löper et al. [14]. In that case, because of the lower extinction coefficient (see Fig. 2(b)), a significantly thicker (302 nm) perovskite layer is needed to achieve current matching. However, because the larger perovskite thickness largely compensates the lower extinction coefficient, the EQE and matched current density value obtained (17.55 mA/cm^2) are similar (graph not shown). This illustrates that the current matching thickness of the perovskite layer is highly dependent on its extinction coefficient. However, the matched current density is much less affected by variations in the optical properties of perovskite.

Optics EXPRESS

3.2 Rear side texture (B)

First, we address reflectance R_3 that occurs only for the weakly absorbed light ($\lambda > 1000$ nm) that is able to pass through the c-Si layer. Note that using a less reflective back reflector would reduce R_3, but not have the desired effect of increasing the device current. Instead, the back reflector should remain highly reflective but scatter the reflected light obliquely. In this way the path length of the weakly absorbed light in c-Si is increased significantly because it traverses the c-Si wafer obliquely and because light confinement is improved due to total internal reflection. This can be achieved using a rear-side texture while keeping the front side flat. This is device B shown in Fig. 3(b). This device was simulated and the resulting absorptances in c-Si and perovskite are shown in Fig. 5. Relative to device A, device B shows a large increase in absorptance of c-Si in the wavelength range 1000 to 1200 nm. In this range c-Si is weakly absorbing and the absorptance is enhanced as a result of the increased path length of this light inside the c-Si. The increased absorptance in c-Si results in an increase in bottom cell current. As mentioned above, all devices shown here have perfect current matching between top and bottom cell. The currents were matched by increasing the perovskite thickness from 140 nm (device A) to 164 nm (device B). This explains the increase in perovskite absorptance and small reduction in c-Si absorptance for $\lambda < 800$ nm. The obtained matched current density is 18.16 mA/cm^2, which is an increase of 5.1% relative to device A.

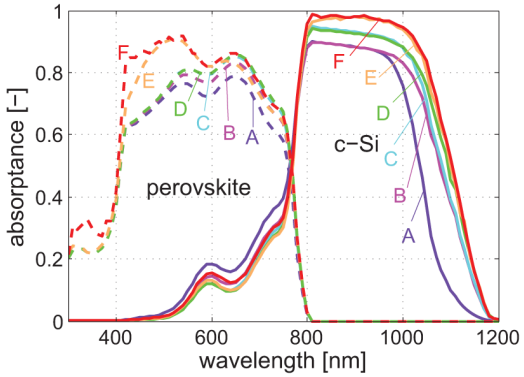

Fig. 5. Simulated absorptances in perovskite and c-Si for current matched tandem device configurations A to F shown in Fig. 3.

3.3 Interlayer (C)

Next we address the reflectance R_2 from the interfaces between perovskite and c-Si. Here an anti-reflective interlayer between top and bottom cell is used to couple more light into the c-Si bottom cell, resulting in device C (see Fig. 3(c)). However, to observe the anti-reflective effect, the material used for this interlayer should, at least in the relevant wavelength range 800 to 1100 nm, have a refractive index n in between that of the ETM ($n \approx 2.3$) and a-Si:H ($n \approx 3.5$). Usually the optical thickness of an anti-reflective coating is tuned to a quarter of the relevant wavelength to exploit interference effects and minimize reflection. In this case interference occurs in the whole optical stack ETM/interlayer/a-Si(p)/a-Si:H(n) and finding the optimum coating thickness requires optical simulations. To find the optimum combination of coating refractive index and thickness we vary both these parameters. Note that the perovskite thickness is adjusted to keep top and bottom cell currents matched for each combination. The resulting matched current density as function of coating index and thickness is shown in Fig. 6. This reveals that a maximum current density of 18.60 mA/cm^2 can be obtained for a coating with $n = 2.8$ and a thickness of 90 nm. Relative to device B this is a further increase in current density of 2.4%. Note that the optimum refractive index of 2.8

Optics EXPRESS

is close to the geometric mean of the indices of ETM and a-Si:H, as expected. Also note that for a 90 nm interlayer thickness, the first order reflection minimum is in the relevant wavelength range 800 to 1100 nm. The appearance of a local maximum for a thicker (250 nm) coating (see Fig. 6) can be explained by the second order reflection minimum moving into this wavelength range. A transparent conductive oxide (TCO) has been used as electrical recombination layer between top and bottom cell [15]. However, the refractive index of most TCO materials is around 2.0, which is much lower than the optically ideal value of 2.8. Also tunnel recombination junctions of highly doped a-Si:H layers have been used [16]. This material has a refractive index around 3.5, which is much higher than the ideal value. However, by alloying a-Si:H with oxygen, its refractive index can be tuned to any value between 3.5 and 2.0, depending on the oxygen content [17]. SiO_x:H is therefore an interesting candidate to be used as interlayer in perovskite/c-Si tandem devices.

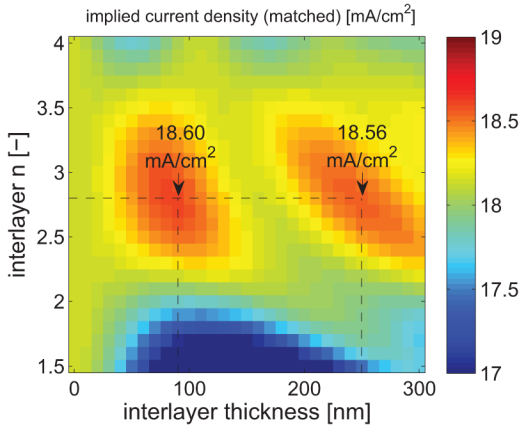

Fig. 6. Simulated matched current density in tandem device C (see Fig. 3(c)) as a function of interlayer thickness and refractive index.

The simulated absorptance in perovskite and c-Si for device C with optimum interlayer is shown in Fig. 5. This reveals that in the wavelength range 800 to 1100 nm the absorptance in c-Si is increased by about 6%. To maintain current matching in top and bottom cell, the perovskite thickness had to be increased further, from 164 nm to 183 nm. This is again accompanied by an increase in the absorptance of perovskite and a small reduction in the absorptance in c-Si for $\lambda < 800$ nm.

For reasons that will become clear in the next section, a device with a very thick (≈10 μm) interlayer was simulated as well. Because the optical thickness of this layer exceeds the coherence length of the incident sunlight, interference is no longer observed [18]. Because of the absence of interference and because we assume that the interlayer is non-absorbing, the simulation result no longer depends on the exact thickness of the interlayer, but only on its refractive index. The gray line in Fig. 7 shows the matched device current density as a function of interlayer refractive index in this limit of large interlayer thickness. This shows that the highest device current density is obtained with an interlayer index of 2.8. This is in agreement with the results shown in Fig. 6. The maximum obtainable current density is however slightly lower (18.47 mA/cm^2) because the thick interlayer does not exploit interference effects.

3.4 Burial layer (D)

An alternative way to reduce reflectance R_2, while keeping the top cell flat, is by using a double side textured c-Si bottom cell with a so-called burial layer on top. This transparent burial layer has a thickness of about 10 μm, which is thick enough to completely cover the

Optics EXPRESS

pyramid texture. Its front side is polished to provide a flat substrate for the perovskite top cell. We assume that the burial layer is non-absorbing and, because its thickness exceeds the coherence length, interference does not play a role. Just like the case of the thick interlayer (section 3.3) the optical performance of this device D depends only on the refractive index of the layer and not on its thickness.

The tandem device with burial layer was simulated for burial layer refractive index values ranging from 1 to 4 and the result is shown in Fig. 7 (green line). In this case the optimum refractive index is 2.0, which is much lower than the optimum index of 2.8 for the thick flat interlayer (gray line). The optimum index is close to the index of ETM, instead of being close to the geometric mean value of the indices of ETM and a-Si:H. This can be explained by the fact that the burial layer's bottom interface has an anti-reflective texture and has a very low reflectance regardless of the refractive index of the burial layer. On the other hand, the burial layer's top interface is flat and its reflectance is minimized when the index of the burial layer is close to that of the ETM. Most TCO materials have a refractive index close to the ideal value of 2.0. A 10 μm thick TCO burial layer would therefore be ideal, provided that the parasitic absorption loss due to free-carrier absorption is sufficiently low. Free-carrier absorption can be kept low by having a low charge carrier concentration. The resulting lower conductivity is not a problem as no lateral conductivity is required in the burial layer.

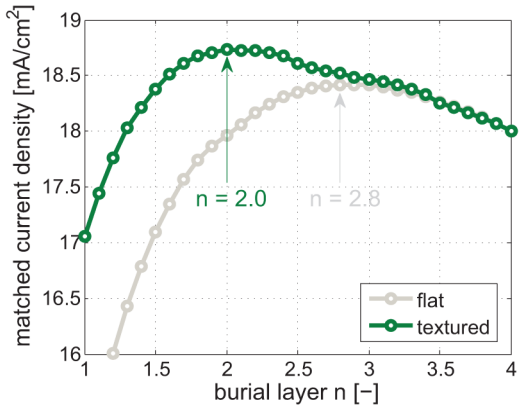

Fig. 7. Simulated matched current density as a function of interlayer/burial layer index. The gray line represents device C in the limit of large interlayer thickness. The green line represents device D.

Device D with burial layer of optimum refractive index reaches a device current density of 18.72 mA/cm^2. Because this is slightly higher than what can be obtained with the flat interlayer (device C), it can be concluded that the burial layer performs slightly better than the flat interlayer. The corresponding absorptance in perovskite and c-Si of device D are indicated in Fig. 5. This shows that the gain relative to device C, although small, originates from increased absorption in c-Si at λ = 1000 to 1200 nm. This indicates that the additional textured interface is beneficial for further increasing the path length of weakly absorbed light inside the c-Si wafer. The perovskite thickness for current matching is 187 nm, which is very similar to the value for device C.

3.5 Front AR coating (E)

The remaining reflectance R_1, originating from the front interfaces, can be reduced by applying a standard anti-reflective coating on top of the ITO, resulting in device E (see Fig. 3(e)). We use an MgF_2 coating that has a refractive index of about 1.38. The wavelength dependent n and k were measured in-house and used in the simulation. The perovskite/c-Si tandem with MgF_2 coating was simulated for a range of MgF_2 thicknesses. For each MgF_2 thickness the perovskite layer thickness was adjusted to achieve perfect current matching. The

Optics EXPRESS

maximum device current density as high as 19.57 mA/cm^2 was obtained for an MgF_2 thickness of 115 nm (see Fig. 8). This in a further increase of 4.5% relative to device D.

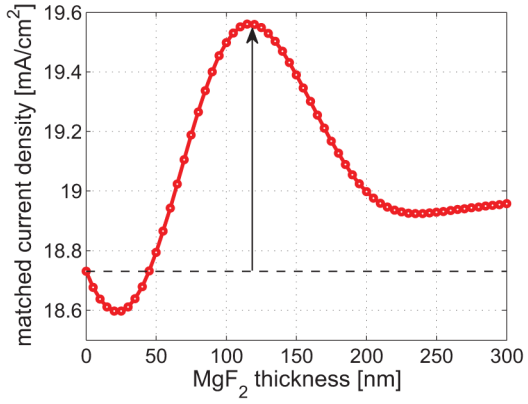

Fig. 8. Simulated matched current density in tandem device E as a function of MgF_2 coating thickness.

The corresponding absorptance in perovskite and c-Si are shown in Fig. 5 (device E). As a result of the reduction of R_1 there is a significant enhancement in perovskite absorptance in the wavelength range 400 to 500 nm. Also the absorptance of c-Si is further enhanced in the 800 to 1100 nm wavelength range. The perovskite layer thickness required for current matching is 182 nm. The same perovskite and c-Si absorptance are shown in Fig. 9, along with the parasitic absorption losses in all other layers and the reflection losses. Comparing this to the results from device A, shown in Fig. 4, it is evident that the total reflectance (white area) is indeed much reduced. Especially R_2 has become negligibly small.

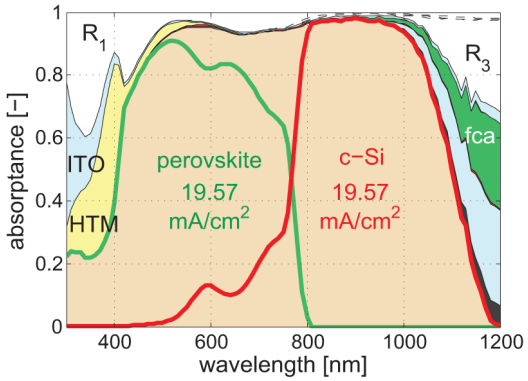

Fig. 9. Simulated absorptance and reflectance of current matched perovskite/c-Si tandem device E.

3.6 Top cell on texture (F)

Finally the perovskite/c-Si tandem device is simulated with a double side textured bottom cell. No burial layer is applied so the perovskite top cell is deposited directly on the pyramid texture (device F shown in Fig. 3(f)). As explained in the introduction, it is difficult to fabricate a working perovskite top cell on this texture. However, device F is simulated in order to assess the potential device current density in case these fabrication issues can somehow be resolved. The simulation result is shown in Fig. 10. This reveals that device F has even lower reflection losses compared to device E. This results in an even higher matched current density of 20.25 mA/cm^2.

Optics EXPRESS

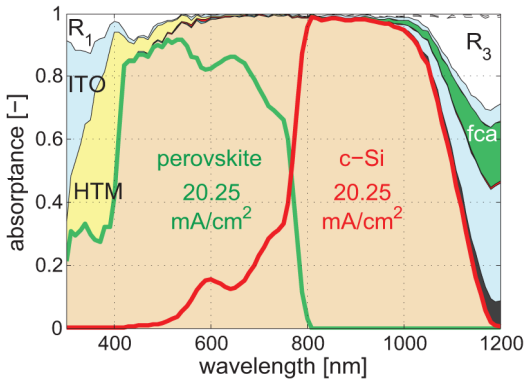

Fig. 10. Simulated absorptance and reflectance of current matched perovskite/c-Si tandem device F.

4. Discussion

The simulation results of devices A to F are summarized in Fig. 11. This figure shows the *total* current density (red), which we define as the sum of the current densities of top and bottom cell. Just like the useful absorption in perovskite and c-Si, the *losses* can be expressed in terms of a current density by integrating them over the AM1.5 spectrum. The dark gray area indicates the total parasitic absorption losses and the light gray areas indicate the reflection loses R_1, R_2 and R_3. Because of conservation of energy, the sum of all contributions is the same for all devices (46.4 mA/cm^2).

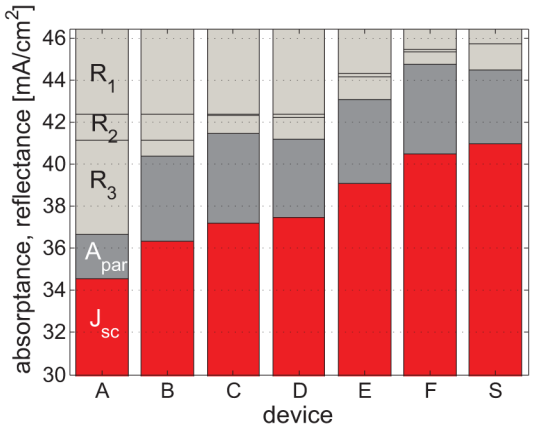

Fig. 11. Useful absorptance (red), parasitic absorptance (dark gray) and reflectance contributions R_1, R_2 and R_3 (light gray) expressed in mA/cm^2 for tandem devices A to F and single junction device S.

Figure 11 shows that flat device A suffers from the largest reflection losses. In device B (with rear texture) R_3 is much reduced. In devices C (with interlayer) and D (with burial layer) R_2 is reduced to nearly zero. In device E (with MgF_2 coating) also R_1 is reduced. The consequence of these systematic reflection reductions obviously is an increased absorptance. This is partly an increase in useful absorption in perovskite and c-Si (red) and partly an increase in parasitic absorption (dark gray).

Going from device A to E, we have shown the route towards high current densities in a perovskite/c-Si tandem device with a flat, easy to fabricate, perovskite top cell. Device E achieves a high current density of 2 × 19.57 mA/cm^2 = 39.14 mA/cm^2, which is an increase of more than 13% relative to device A. Nonetheless, in device F, with the perovskite top cell

Optics EXPRESS

deposited directly on a textured surface, reflection losses are even lower. This means that if the deposition of a high quality perovskite top cell on a textured surface would become feasible in the future, an even higher current density of 2 × 20.25 mA/cm^2 = 40.50 mA/cm^2 could potentially be reached.

Finally, we compare these current densities to that of the silicon heterojunction solar cell shown in Fig. 1. We label this single junction device 'device S' and show its current densities in Fig. 11 (right most bar). The total current density of device S (40.9 mA/cm^2) is even higher than for any of the tandem devices. Figure 11 reveals that this is not due to lower reflection losses, but due to lower parasitic absorption losses in device S. All perovskite/c-Si tandem devices suffer from parasitic absorption losses in the perovskite top cell, especially in HTM and to a lesser extent also free carrier absorption in perovskite. These losses do not play a role in single junction device S. Note that parasitic absorption losses in HTM can to a large extent be avoided by inverting the top cell structure, i.e. having the ETM in front and the HTM behind the perovskite layer. The bottom cell structure then has to be inverted correspondingly.

5. Conclusions

Our model GENPRO4 has proven a powerful tool for optical simulation of perovskite/c-Si tandem solar cells. The goal of our work was to develop a new monolithic perovskite/c-Si tandem device architecture with a flat perovskite top cell, but with a minimum of optical losses. Our simulations showed that a tandem device based on a double side polished c-Si wafer (device A) suffers from large reflection losses and consequently has a relatively low matched device current density of 17.28 mA/cm^2. Reflection losses were then reduced systematically by applying a rear side texture, a front side texture with burial layer and an MgF_2 anti-reflective coating. This results in a more than 13% higher matched device current density of 19.57 mA/cm^2 (device E), which is very high considering that the perovskite top cell is flat. Comparing these results to a tandem device with perovskite top cell on texture (device F) or single junction c-Si solar cell (device S) revealed that in principle there is room, although limited, to increase the device current density even further by further reducing reflection and parasitic absorption losses.

Acknowledgments

The authors would like to thank Fai Tong Si of Delft University of Technology for performing AFM measurements. In addition we thank Dong Zhang of Energy research Centre Netherlands for fruitful discussions.